Network Coded LDPC Code Design for a Multi-Source Relaying System

Jun Li, *Member, IEEE*, Jinhong Yuan, *Member, IEEE*, Robert Malaney, *Member, IEEE*, Marwan H. Azmi, *Student Member, IEEE*, and Ming Xiao, *Member, IEEE*

***Abstract*—We investigate LDPC code design for a multi-source single-relay system, with uniform phase-fading Gaussian channels. We specifically consider the asymmetric channels for multiple sources, where the channel condition for each source in the system is different. We focus on LDPC code design when network coding (NC) at the relay is utilized. For the asymmetric sources, we firstly introduce a *binary field rate splitting theorem* which is used to discover an appropriate NC scheme at the relay. This NC scheme is then used to determine the achievable rates of each source and the whole system. These steps assist us in the development of the main contribution of our work, namely, network coded multi-edge type LDPC (NCMET-LDPC) code design. Extrinsic mutual information transfer (EXIT) chart analysis is utilized to optimize the code profiles. Our results demonstrate two key points.** (1) **From the whole system point of view, our NCMET-LDPC codes achieve better error performance than that of LDPC codes designed for the system without NC.** (2) **As a consequence of the *binary field rate-splitting theorem*, our NCMET-LDPC codes also guarantee better error performance of each asymmetric source. The improvement in error performance is typically about** 0.3 **dB relative to a system without NC.**

***Index Terms*—Multi-source relaying, multi-edge type LDPC codes, network coding, extrinsic mutual information transfer (EXIT).**

I. Introduction

COOPERATIVE communications systems composed of one source, one relay, and one destination ($1-1-1$ systems) have been widely studied, and the achievable rates in such systems have been developed [1, 2]. In addition, design of the channel capacity-approaching codes, *e.g.* low-density parity-check (LDPC) codes [3–5] which approach the achievable rates of $1-1-1$ systems, have been investigated [6–10]. However, in emerging networks, such as cellular relaying networks, a relay will be shared by multiple sources and utilized to forward messages to the common destination, *e.g.* a base station. These networks, which can be modeled as $M-1-1$ systems, composed of M sources, one relay, and one destination, have attracted much attention recently in the research community.

In the $M-1-1$ systems with the DF (Decode-and-Forward) protocol, the relay decodes the messages of all the sources. There are several information processing methods at the relay. One of these is the separate processing (SP) method, where the relay generates the extra redundant messages for each source individually without combining them with the messages of the other sources. Subsequently, the relay forwards the messages to the destination in order to facilitate the decoding of the source's messages. A second method of processing at the relay is the network coding (NC) method [11]. In this method, the relay generates the extra redundant messages by combining the messages of all the sources according to a specific NC scheme. In NC schemes the relay generates the extra redundant messages in either the complex field (it is actually a kind of signal (symbol) superposition technique) [12, 13], or Galois field [14, 15]. It has been proved that [12, 14] under the fading channels, the $M-1-1$ system, with either complex field NC or Galois field NC, achieves a higher diversity gain than that with SP for each source.

Relative to complex field NC, one advantage of Galois field NC is the joint design with the channel coding. In [16], LDPC-like codes are jointly designed with Galois field NC in a multiple source system, where Rayleigh fading channels are considered and each source is alternately utilized as the relay for the other sources. In [17], turbo codes are jointly designed with Galois field NC for a $2-1-1$ system assuming Rayleigh fading channels. However, these two works do not consider the optimization of the code profiles in fading channels. For the $M-1-1$ systems with AWGN channels, the works of [18, 19] explore code optimization by combining the Galois field NC with bilayer LDPC codes [6]. However, there are two main limitations of [18, 19]. Firstly, these works do not consider the fact that the system achievable rate is changed after applying Galois field NC at the relay. Secondly, these works only focus on code design in the special case where the source-to-relay channels have the same achievable rates, and the source-to-destination channels have the same achievable rates. In this work, we will address these two important issues.

We consider the code design for asymmetric channel conditions of multiple sources, where the channel signal-to-noise ratios (SNR) and the achievable rates for all the sources are different. We consider only Galois field NC, henceforth simply

Manuscript received May 11, 2010; revised October 26, 2010 and February 16, 2011; accepted March 3, 2011. The associate editor coordinating the review of this paper and approving it for publication was M. C. Valenti.

The work in this paper is partially supported by the Australian Research Council (ARC) Discovery Projects DP110104995, and is partially supported by the Swedish Research Council (VR).

J. Li, J. Yuan, and R. Malaney are with the School of Electrical Engineering and Telecommunications, University of New South Wales, Sydney, NSW 2052, Australia (e-mail: {jun.li, j.yuan, r.malaney}@unsw.edu.au).

M. H. Azmi is with the Faculty of Electrical Engineering, Universiti Teknologi Malaysia. He is currently on a study leave and working toward his Ph.D. at the University of New South Wales, Australia (e-mail: marwan@student.unsw.edu.au).

M. Xiao is with the ACCESS Linnaeus Center, School of Electrical Engineering, Royal Institute of Technology, Sweden (e-mail: ming.xiao@ee.kth.se).

Digital Object Identifier 10.1109/TWC.2011.032411.100794

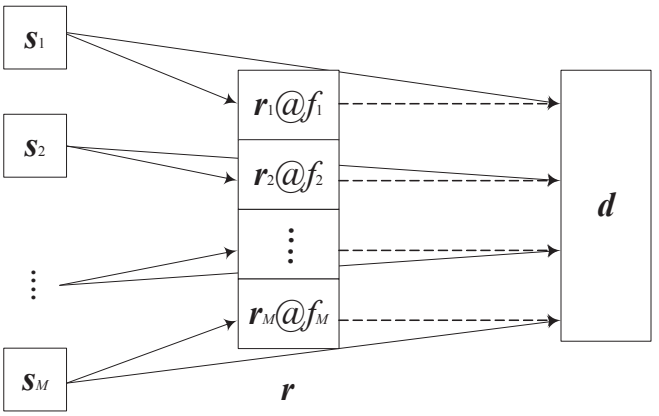

Fig. 1. The working mode of an FDMA $M-1-1$ system. The relay r has M parts $r_1, \cdots, r_M$ receiving and transmitting at $f_1, \cdots, f_M$, respectively.

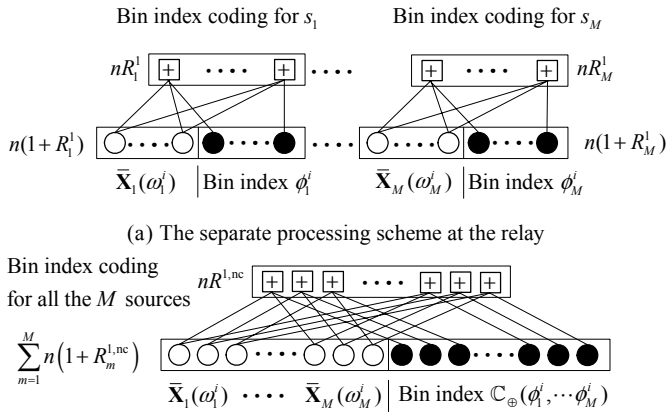

(a) The separate processing scheme at the relay

(b) The network coding scheme at the relay

Fig. 2. The comparison of the separate processing (SP) scheme and the network coding (NC) scheme. Figure (a) shows the separate processing scheme at the relay. The relay generates the bin indexes for each source individually. Note that all the variable nodes associated with the bin indexes $\phi_1^i,\cdots,\phi_M^i$ are degree one. Figure (b) shows the network coding scheme at the relay. The relay jointly generates a bin index for all the sources according a network coding scheme $\mathbb{C}_\oplus$. Note that all the variable nodes associated with the bin index $\mathbb{C}_\oplus(\phi_1^i,\cdots,\phi_M^i)$ are degree one.

referred to as NC. We will adopt an $M-1-1$ system in which sources transmit their information via frequency division multiple access (FDMA). Such an access scheme is consistent with emerging LTE standard [20]. Our specific contribution for such a system are as follows. (i) We propose a *binary field rate-splitting theorem* to determine how many network coded digits are allocated to each asymmetric source in an NC scheme. (ii) We consider the design of network coded LDPC codes and propose a novel network coded multi-edge type LDPC code structure (NCMET-LDPC). In our design of NCMET-LDPC codes, the relay generates the network coded parity check digits from the messages of all the sources. Contrary to other code designs (*e.g.* [18, 19]), the structure of the NCMET-LDPC codes we design can be applied to asymmetric channels where all the channels possess different conditions. (iii) EXIT analysis [21–23] is utilized to optimize the NCMET-LDPC code profiles, with the *binary field rate-splitting theorem* being used as a constraint.

The rest of this paper is organized as follows. Section II sets up the system model and presents the achievable rate analysis for the system with SP. Section III derives the *binary field rate-splitting theorem*, based on which the achievable rate of the system with NC is analyzed. Section IV focuses on the methodology of the NCMET-LDPC code design. Section V analyzes the EXIT property of the NCMET-LDPC codes and proposes the optimization criterions of the codes. Section VI provides our simulation results of the bit error performance, and Section VII concludes the paper.

II. System Model and Preliminaries

Consider an $M-1-1$ system with M sources, one relay and one destination, where sources $s_1, \cdots, s_M$ broadcast their messages to the destination d simultaneously. In the same time, a full-duplex relay r tries to decode the messages of all the sources and forwards extra redundant messages to the destination. Suppose that all the sources access the channels using frequency division multiple access (FDMA). The relay receives and transmits in all the frequencies utilized by the sources. Specifically, as shown in Fig. 1, the m-th source s_m, $m = 1, \cdots, M$, transmits its messages in the frequency band f_m, the relay r has M parts, *i.e.* $r_1, \cdots, r_M$, which receive and transmit signals at $f_1, \cdots, f_M$, respectively, and the destination d also receives signals at these M orthogonal frequency bands. We assume that both the sources and the relay have the same block length n. We focus on the phase-fading channels [1] with AWGN, and suppose that the relay does not know the phase of each source-to-destination channel. Therefore, there is no coherent superposition between the signals of a source and the relay.

The physical locations of the sources are assumed to be randomly distributed around the relay r. The distance between s_m and r is supposed not to exceed the distance between s_m and d. We denote the distance between s_m and r, the distance between s_m and d, and the distance between r and d as d_m^{sr}, d_m^{sd} and d^r, respectively. Note that $d_m^{sr} \leq d_m^{sd}$ for all m. The pass losses of all the channels are associated with their distances with the same attenuation exponent α. Therefore, the channel coefficients between s_m and r, s_m and d, r and d are $h_m^{sr} = \frac{e^{j\phi_m^{sr}}}{\sqrt{(d_m^{sr})^\alpha}}$, $h_m^{sd} = \frac{e^{j\phi_m^{sd}}}{\sqrt{(d_m^{sd})^\alpha}}$, and $h_m^{rd} = \frac{e^{j\phi_m^{rd}}}{\sqrt{(d^r)^\alpha}}$, respectively. Note that ϕ_m^{sr}, ϕ_m^{sd} and ϕ_m^{rd} are the received signal phases between the s_m-to-r_m channel, the s_m-to-d channel, and the r_m-to-d channel, respectively. All receivers are assumed to have the same noise power N.

Since the M sources access the relay r and the destination d via FDMA, the $M-1-1$ system can be viewed as M independent parallel $1-1-1$ systems operating at M frequency bands. In this view, the relay separately processes M sources' messages and forwards M sources' bin indexes at M frequency band, respectively. Therefore, we term this process as separate processing (SP). Let us consider the m-th $1-1-1$ system composed of s_m, r_m and d. The conventional binning scheme [1, 2] for analyzing relay channels can be utilized to obtain the achievable rate. In this scheme, the message set of s_m, $\{1, \cdots, 2^{nR_m}\}$, is randomly partitioned into $2^{nR_m^1}$ bins ($R_m^1 \leq R_m$) of size $2^{n(R_m - R_m^1)}$, where R_m and R_m^1 are the transmission rates of s_m's messages and the

messages' bin indexes at the relay, respectively. According to [1], the source s_m transmits the i-th message ω_m^i with power P_m, and the relay r_m transmits the bin index ϕ_m^i with power P_{1m}. The SP scheme at the relay is shown in Fig. 2(a), where the Tanner graph for each source's bin index encoder is illustrated. Suppose that the messages ω_m^i and ϕ_m^i are encoded by $\bar{\mathbf{X}}_m(\omega_m^i)$ and $\mathbf{X}_{1m}(\phi_m^i)$ via random codebooks of sizes 2^{nR_m} and $2^{nR_m^1}$, respectively. In the m-th frequency band, the destination receives the i-th signal frame as $\mathbf{Y}_m^i = \bar{\mathbf{X}}_m(\omega_m^i) + \mathbf{X}_{1m}(\phi_m^i) + \mathbf{n}_m^i$, where $\mathbf{n}_m^i$ is the noise vector observed by the destination at the m-th frequency band. Then the achievable rate of the $1-1-1$ system with uniform phase fading channels can be written as [1]

$$R_m = \min\left\{\log\left(1+\frac{P_m}{(d_m^{sr})^\alpha N}\right), \log\left(1+\frac{P_m}{(d_m^{sd})^\alpha N}+\frac{P_{1m}}{(d^r)^\alpha N}\right)\right\}. \quad (1)$$

The first item on the right hand side (RHS) of (1) is the mutual information between s_m and r_m, *i.e.* $I(s_m; r_m)$. We denote R_m^+ as the maximum rate of s_m's messages received at r_m, then $R_m^+ = I(s_m; r_m)$. The second item on the RHS of the equation is the mutual information between $\{s_m, r_m\}$ and d, *i.e.* $I(s_m, r_m; d)$. At the destination, we firstly decode the bin index messages from the relay by treating s_m's messages as noise, and then decode the s_m's messages by concealing the bin index messages. Thus, we obtain the maximum rate of the bin index as $R_m^1 = \log\left(1+\frac{P_{1m}}{(d^r)^\alpha(P_m/(d^{sd})^\alpha+N)}\right)$, and the maximum rate of s_m's messages at the destination as $R_m^- = \log\left(1+\frac{P_m}{(d^{sd})^\alpha N}\right)$.

The achievable rate of the $M-1-1$ system with SP at the relay can be derived under the following constraints: (a) There is no optimization of the sources' power allocations due to their distributed nature. (b) At the relay r, power allocation is optimized between the M parts of the relay, subject to a total power constraint given by $\sum_{m=1}^M P_{1m} \le P_{10}$, where P_{10} is the total power at the relay. The achievable rate of the $M-1-1$ system with the SP method is the maximal summation of the rates of all the $1-1-1$ systems among various power allocation schemes at the relay r, *i.e.*

$$\begin{aligned} R &= \max_{P_{11},\cdots,P_{1M}} \sum_{m=1}^M \min\left\{R_m^+, R_m^1 + R_m^-\right\} \\ &\le \max_{P_{11},\cdots,P_{1M}} \min\left\{\sum_{m=1}^M R_m^+, \sum_{m=1}^M R_m^1 + \sum_{m=1}^M R_m^-\right\}. \end{aligned} \quad (2)$$

To maximize R, the water filling principle [24] can be utilized to enhance the total rate of the bin indexes *i.e.* $\sum_{m=1}^M R_m^1$ at the relay. This is a consequence of the use of the M parallel r-to-d channels. Different from the traditional usage of this principal, according to (2), extra constraints $R_m^1 \le R_m^+ - R_m^-$, $m = 1, \cdots, M$, should be satisfied to optimize R in (2). After the conventional water filling algorithm, if in the m-th $1-1-1$ system, the P_{1m} is so large that there is $R_m^1 > R_m^+ - R_m^-$, then the rate of the m-th $1-1-1$ system is bounded by R_m^+. This means that letting $R_m^1 > R_m^+ - R_m^-$ will waste the power of the relay. We need to reduce the power P_{1m} to make sure that $R_m^1 = R_m^+ - R_m^-$ in order to save the power. The saved power from the m-th $1-1-1$ system should be reallocated to other $1-1-1$ systems, *e.g.* the m'-th $1-1-1$ system, $m' \ne m$, in which $R_{m'}^1 < R_{m'}^+ - R_{m'}^-$. Therefore, to achieve the maximum rate of the $M-1-1$ system, we need to make sure that $R_m^1 \le R_m^+ - R_m^-$ for all m. Then we obtain a *constrained water filling* (CWF) algorithm at the relay for the $M-1-1$ system.

Theorem 1: In the $M-1-1$ system with SP, the power allocation at the relay that obtains the achievable rate is

$$P_{1m} = \begin{cases} 0, & \frac{\log e}{\tau} \le \frac{1}{p_m} \\ \frac{\log e}{\tau} - \frac{1}{p_m}, & \frac{1}{p_m} < \frac{\log e}{\tau} < d_m P_m + \frac{1}{p_m} \\ d_m P_m, & \frac{\log e}{\tau} \ge d_m P_m + \frac{1}{p_m}, \end{cases} \quad (3)$$

where $d_m = \left(\frac{d^r}{d_m^{sd} d_m^{sr}}\right)^\alpha \left((d_m^{sd})^\alpha - (d_m^{sr})^\alpha\right)$, $p_m = \frac{1}{(d^r)^\alpha (P_m/(d_m^{sd})^\alpha + N)}$, $\tau = \frac{W \log e}{\sum_{w=1}^W \frac{1}{p_w} + P_{10}}$, and $W \le M$ is the number of sources such that $\log e/\tau - 1/p_m > 0$.

Proof: Add the constraints $R_m^1 \le R_m^+ - R_m^-$, $m = 1, \cdots, M$, to the proof of conventional water filling algorithm [24], and then we can easily get (3). ■

Regarding LDPC code design for the $M-1-1$ system with SP, since the $M-1-1$ system can be split into M parallel $1-1-1$ systems, we directly apply the design methodology of bilayer multi-edge type LDPC (BMET-LDPC) codes [7] to each $1-1-1$ system individually. That is, when the relay obtains the messages of a source, it only generates the parity check digits for the source based on the source's own messages. Coupling such a code design to the discussion given above, we see how the achievable rates of the $M-1-1$ system with SP can be readily determined. The achievable rate and the LDPC code design in the system with SP will be used as the benchmarks for the comparisons with the achievable rate and network coded multi-edge type LDPC (NCMET-LDPC) codes in the system with NC.

III. Achievable Rate for the System with NC

In the $M-1-1$ system with NC, the bin index messages $\phi_1^i, \cdots, \phi_M^i$ are firstly generated at the relay r from the received signals at all the frequency bands. Then these bin index messages are encoded by a network coding scheme $\mathbb{C}_\oplus$ before retransmission by r. The network coded signals can be seen as the bin index of the super block composed of the blocks from all the sources. We denote the network coded bin index as $\mathbb{C}_\oplus(\phi_1^i, \cdots, \phi_M^i)$. Then the network coded bin index is encoded as $\mathbf{X}_{10}(\mathbb{C}_\oplus(\phi_1^i, \cdots, \phi_M^i))$ and transmitted by r. At the destination decoder, the successive decoding is applied. More specifically, $\mathbb{C}_\oplus(\phi_1^i, \cdots, \phi_M^i)$ is firstly decoded by treating $\bar{\mathbf{X}}_1(\omega_1^i), \cdots, \bar{\mathbf{X}}_M(\omega_M^i)$ as noise. Then $\bar{\mathbf{X}}_1(\omega_1^i), \cdots, \bar{\mathbf{X}}_M(\omega_M^i)$ are decoded after performing successive interference cancelation of the bin index signal from the receiving signal. In the following, we shall show how the $M-1-1$ system with NC obtains a higher achievable rate than that with SP. Note that the superscript 'nc' is utilized for all the rates in the system with NC.

Before presenting the achievable rate, we firstly present a *binary field rate-splitting theorem*. In the $M-1-1$ system with NC, coded digits from the sources are superimposed in the binary field and utilized in the generation of network coded

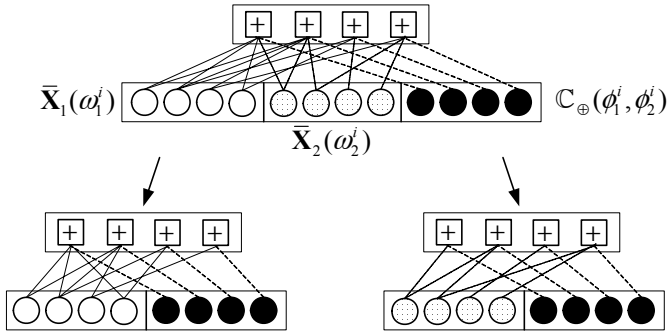

Fig. 3. The decomposition of the Tanner graph into two sub-graphs in a two-source case. The process of decomposition follows the method in Appendix A.

bin index $\mathbb{C}_\oplus(\phi_1^i, \cdots, \phi_M^i)$ at the relay. We propose the *binary field rate-splitting theorem* in order to determine the number of the digits in $\mathbb{C}_\oplus(\phi_1^i, \cdots, \phi_M^i)$ allocated to each source.

Since all the blocks have the length n, we have the number of digits in $\mathbb{C}_\oplus(\phi_1^i, \cdots, \phi_M^i)$ is $nR^{1,\text{nc}} = n\sum_{m=1}^M R_m^{1,\text{nc}}$, in which $nR_m^{1,\text{nc}}$ is the number of digits allocated to the m-th source's bin index signal $\mathbf{X}_{1m}(\phi_m^i)$. Different from an SP scheme, in the NC scheme the number of digits allocated to $\mathbf{X}_{1m}(\phi_m^i)$ is not straightforward because each coded digit in $\mathbb{C}_\oplus(\phi_1^i, \cdots, \phi_M^i)$ is generated from multiple sources. We call $nR_m^{1,\text{nc}}$ the effective number of digits for s_m at the relay r. The determination of $nR_m^{1,\text{nc}}$ can be found by considering the Tanner graph of the NC scheme. Fig. 2 shows the Tanner graph of the coding schemes in the $M-1-1$ system with the SP scheme and the NC scheme. Particulary in Fig. 2(b) we see that the network coding scheme $\mathbb{C}_\oplus$ generates the parity checks for all the sources. The variable nodes for s_m are associated with the digits in both the network coded bin index $\mathbb{C}_\oplus(\phi_1^i, \cdots, \phi_M^i)$ and s_m's codeword $\bar{\mathbf{X}}_m(\omega_m^i)$. Note that the variable nodes with black circles in Fig. 2(b) are associated with the digits in $\mathbb{C}_\oplus(\phi_1^i, \cdots, \phi_M^i)$. We now present the *binary field rate-splitting theorem*.

Theorem 2: In an $M-1-1$ system with NC, assuming the bin index signals $\phi_1^i, \cdots, \phi_M^i$ at the relay are network coded by a coding scheme $\mathbb{C}_\oplus$ and assuming the relay transmits the network coded signal $\mathbb{C}_\oplus(\phi_1^i, \cdots, \phi_M^i)$ to the destination. For successive decoding, the effective number of digits allocated to s_m, (*i.e.* the equivalent number of the bin index digits that are used at the destination for the decoding of s_m), $nR_m^{1,\text{nc}}$, is computed as

$$nR_m^{1,\text{nc}} = \sum_{j=1}^{d_c} \sum_{j_m=0}^{j} \frac{j_m}{j} \vartheta_m^j. \tag{4}$$

Here, $j = 1, 2, \cdots, d_c$, is the degree of the check nodes associated with $\mathbb{C}_\oplus$, j_m is the number of edges that emanate from a degree-j check node and are connected to the variable nodes associated with the digits in $\bar{\mathbf{X}}_m(\omega_m^i)$, and ϑ_m^j is the number of the degree-j check nodes with the j_m edges connected to the variable nodes associated with the digits in $\bar{\mathbf{X}}_m(\omega_m^i)$.

Proof: See Appendix A.

To have a better understanding of *Theorem 2*, we provide below an example for a two-source case.

Example: Consider a two-source case where each source has 4 bits of information. The digits in the two sources are combined according to the network coding scheme $\mathbb{C}_\oplus$ shown in Fig. 3. The network code produces 4 coded digits. According to Appendix A, we split the whole graph into two subgraphs as shown in Fig. 3.

In the example, there are $nR^{1,\text{nc}} = nR_1^{1,\text{nc}} + nR_2^{1,\text{nc}} = 4$ check nodes and we can easily determine their degrees as $j = 5, 6, 4, 4$. In the successive decoding scheme, both the variable nodes associated with the digits in $\mathbb{C}_\oplus(\phi_1^i, \cdots, \phi_M^i)$ and the edges connected to them are deleted from the graph. This is because $\mathbb{C}_\oplus(\phi_1^i, \cdots, \phi_M^i)$ is decoded firstly at the destination. In this case, we get that $j = 4, 5, 3, 3$, $j_1 = 3, 3, 2, 1$, and $j_2 = 1, 2, 1, 2$. Therefore, the effective numbers of digits for the two sources are $nR_1^{1,\text{nc}} = 3/4 + 3/5 + 2/3 + 1/3 = 2.35$, and $nR_2^{1,\text{nc}} = 1/4 + 2/5 + 1/3 + 2/3 = 1.65$, respectively. ■

We now turn to the achievable rate for the $M-1-1$ system with NC. Recall that in the $M-1-1$ system with SP, the achievable rate is obtained by the *constrained water filling algorithm* with the constraints $R_m^1 \le R_m^+ - R_m^-$ met by the power allocation at the relay r. However, in the system with NC, the bin index signals for all the sources are combined according to the NC scheme, and the coded bin index signals are transmitted in the M parallel r-to-d channels. In this case, the constraints $R_m^1 \le R_m^+ - R_m^-$ are satisfied by the rate allocation (with the network coding scheme $\mathbb{C}_\oplus$) rather than the power allocation. Therefore, in the system with NC, we can apply the conventional water filling algorithm to the relay r to maximize $\sum_{m=1}^M R_m^{1,\text{nc}}$ without any extra power constraint. Obviously, the value of $\sum_{m=1}^M R_m^{1,\text{nc}}$ achieved by the conventional water filling algorithm is larger than $\sum_{m=1}^M R_m^1$ achieved by the constrained water filling algorithm. After obtaining the optimal $\sum_{m=1}^M R_m^{1,\text{nc}}$ by the conventional water filling algorithm, we can design the coding scheme $\mathbb{C}_\oplus$ to guarantee that

$$R^{\text{nc}} = \min\left\{\sum\nolimits_{m=1}^M R_m^+,\ \sum\nolimits_{m=1}^M R_m^{1,\text{nc}} + \sum\nolimits_{m=1}^M R_m^-\right\}. \tag{5}$$

Now we compare the achievable rates in the $M-1-1$ system with SP and NC. We conclude that if R^{nc} is dominated by the first item on the RHS of (5), the system with NC has the same achievable rate as that of the system with SP. If, on the other hand, R^{nc} is dominated by the second item on the RHS of (5), the system with NC can obtain a higher achievable rate than that of the system with SP.

A. Numerical Results

We now provide numerical results for the achievable rates for the $M-1-1$ system with SP and NC. We consider an example of the system as shown in Fig. 4 with $M = 5$ and an attenuation exponent $\alpha = 2$. Successive decoding is applied at the destination. All sources are randomly distributed in a circle with radius 0.5, where distance between the center of the circle and d is normalized to 1. We also assume that the initial position of r is at the center of the circle, and can only move along the line from the center of the circle to d. The value of d_m^{sr} is uniformly distributed in the range $(0, 0.5)$ and the angle φ_m is uniformly distributed in the range $(0, 2\pi]$ when the relay is at its initial position. We consider the total

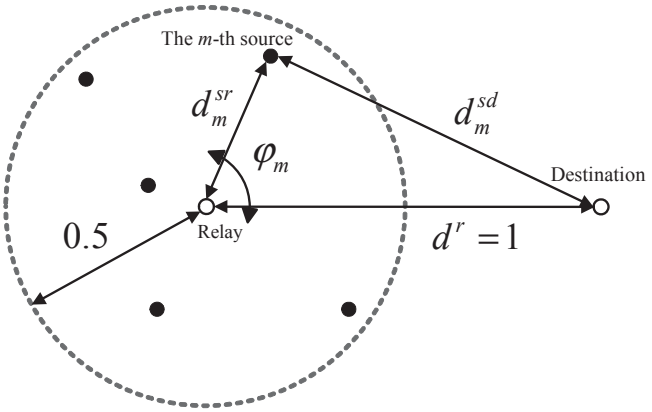

Fig. 4. The geographical distributions of the sources, the relay and the destination. The distance between the relay and the destination is 1. All the sources are randomly distributed in a circle with radius 0.5.

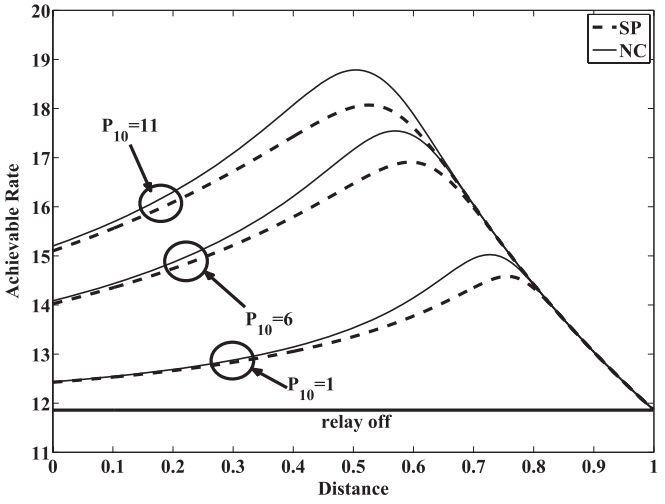

Fig. 5. The achievable rate as a function of distance. The power of each source is uniformly distributed from 1 to 10. The distance is that between r and the center of the circle.

power of r as $P_{10} = 1, 6, 11$ and the noise power spectral densities at all the receivers are all set to $N = 1$. We study the achievable rates of the $M-1-1$ system with SP and NC under various locations of r.

Fig. 5 shows the achievable rates of the system with 2 different power allocation schemes, which are outlined below. (1) Separate processing with constrained water filling algorithm (SP); (2) Network coding with traditional water filling algorithm plus the binary field rate-splitting approach (NC). In the simulation, we assume that the power of each source is uniformly distributed from 1 to 10. From the simulations, we can see that the achievable rate of the system with NC is always greater than or equal to that of the system with SP. In addition, when relay is closer to the destination, the SP scheme and the NC scheme have the same rate. This is because that when relay-to-destination channel is good, the constraint water filling algorithm is equivalent to the traditional water filling algorithm.

IV. Network Coded Multi-Edge Type LDPC Codes

In this section we propose a novel code structure for $M-1-1$ systems, named NCMET-LDPC codes, to approach the achievable rate. The methodology relating to the design of the multi-edge type LDPC codes can be applied to the code design of systems with asymmetric channels. In our system, all the channels may have different achievable rates, and all the transmitted symbols are modulated by BPSK. In our code design we do not consider the error propagation in the s-to-r channels and r-to-d channels. That is, r can successfully decode the messages from all the sources, and d can successfully decode the bin index messages from r. Note that in the code design, we choose the code rates to be the same as the corresponding achievable rates. In the following code design, we denote R with different superscripts as the code rates. We first review the code structure of the multi-edge type LDPC codes.

A. Multi-edge Type LDPC Codes

The principle of multi-edge type LDPC codes is to introduce more than one edge type to the Tanner graph [5]. A multi-edge type ensemble is determined by the degree types of both the check nodes and the variable nodes in the Tanner graph. From a check node point of view, its degree type contains one vector called the edge degree. This is a vector of integers of length n_l, where n_l is the number of edge types. The i-th entry of this vector records the number of edges of the i-th type connected to this check node. The degree type of a variable node has two vectors. The first vector, called the received degree vector, represents the received distribution. The length of this vector is n_τ, where n_τ is the number of different channels over which a signal may be transmitted. The second vector, called edge degree vector, has the similar definition as that of a check node. The length of this vector is n_l.

The multi-edge type ensemble can be specified through two polynomials, one is associated to variable nodes, and the other is associated to check nodes. The polynomials are given by $v(\mathbf{r}, \mathbf{x}) = \sum v_{\mathbf{b},\mathbf{d}} \mathbf{r}^{\mathbf{b}} \mathbf{x}^{\mathbf{d}}$ and $\mu(\mathbf{x}) = \sum \mu_{\mathbf{d}} \mathbf{x}^{\mathbf{d}}$, where $\mathbf{d} = [d_1, d_2, \cdots, d_{n_l}]$ and $\mathbf{b} = [b_0, b_1, \cdots, b_{n_\tau}]$ are the edge degree and the received degree vectors with a length n_l and $n_\tau + 1$, respectively. Note that in vector $\mathbf{b}$, the first element b_0 is utilized to indicate punctured variables. Correspondingly, $\mathbf{x} = [x_1, \cdots, x_{n_l}]$ and $\mathbf{r} = [r_0, r_1, \cdots, r_{n_\tau}]$ denotes variable vectors related to $\mathbf{d}$ and $\mathbf{b}$, respectively, and $\mathbf{x}^{\mathbf{d}} = \prod_{j=1}^{n_l} x_j^{d_j}$ and $\mathbf{r}^{\mathbf{b}} = \prod_{j=0}^{n_\tau} r_j^{b_j}$. The coefficients $v_{\mathbf{b},\mathbf{d}}$ and $\mu_{\mathbf{d}}$ are non-negative reals, which correspond to the percentage of variable nodes with type ($\mathbf{b}$, $\mathbf{d}$) and check nodes with type ($\mathbf{d}$), respectively. For more details on multi-edge type LDPC codes please refer to [5].

B. Structure of NCMET-LDPC Codes

The structure of the NCMET-LDPC codes is shown in Fig. 6. The Tanner graph of Fig. 6 contains a lower part, representing M LDPC codes for the M sources, and an upper part representing the network code at the relay. In Fig. 6, the circles in different rectangles represent the variable nodes associated with the digits of different sources, the boxes in different rectangles of the lower graph represent the check nodes within different sources themselves, and the boxes in

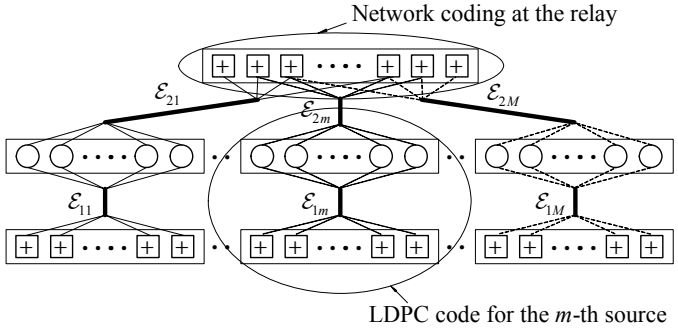

Fig. 6. The code structure of NCMET-LDPC codes.

the rectangles of the upper graph represent the network coded check nodes within the relay r. Note that here we consider the successive decoding scheme, that is, we assume that (ϕ_1^i, $\cdots$, ϕ_M^i) can be recovered firstly. Thus, the variable nodes associated with the digits in $\mathbb{C}_\oplus(\phi_1^i, \cdots, \phi_M^i)$ and the edges connected to them can be deleted from the Tanner graph. We represent the different edge types as $\mathcal{E}$ with different subscripts. For example, the edge type of the lower graph of s_m is denoted as $\mathcal{E}_{1m}$ and the edge type of the upper graph of s_m is denoted as $\mathcal{E}_{2m}$.

Following the same design methodology of conventional bilayer LDPC codes in the $1-1-1$ system, the multi-edge type LDPC code design for an $M-1-1$ system begins with the optimization of the lower graph in Fig. 6 at rates $R_1^+, \cdots, R_M^+$ for $s_1, \cdots, s_M$, respectively. The lower graph ensemble of the multi-edge type LDPC codes for s_m is represented by $v_m(\mathbf{r},\mathbf{x}) = r_1 \sum_{d_{1m}=1}^{d_{v1,m}} v_{[0,1],[d_{1m}]} x_{1m}^{d_{1m}}$ and $\mu_m(\mathbf{x}) = \sum_{d_{1m}=1}^{d_{c1,m}} \mu_{[d_{1m}]} x_{1m}^{d_{1m}}$, where r_1 is the second element of the vector $\mathbf{r}$ and $\mu_{[d_{1m}]}$ is the fraction of degree-d_{1m} check-nodes within the lower graph corresponding to s_m. Corresponding to the polynomials of multi-edge type LDPC codes, we have the vector $\mathbf{b} = [0,1]$, which means that all variable nodes associated with the digits of s_m are transmitted through the $s_m \to r_m$ channel ($b_1 = 1$) at rate R_m^+ and there are no punctured variables ($b_0 = 0$) in the codeword of the m-th lower graph, *i.e.* the lower graph for s_m. We have vector $\mathbf{d} = [d_{1,m}]$ which contains only one element d_{1m} since there is only one edge type for each source's code. We use d_{1m} to represent both the degree of variable nodes (maximum value $d_{v1,m}$) and the degree of check nodes (maximum value $d_{c1,m}$) belonging to s_m. Since all the blocks transmitted by s_m and r_m have the same length n, the value $v_{\mathbf{b},\mathbf{d}} n$ is the number of variable nodes of type $(\mathbf{b},\mathbf{d})$ and $\mu_{\mathbf{d}} n$ is the number of check nodes of the type $(\mathbf{d})$ in the lower graph. The code rate of m-th lower graph is $R_m^+ = 1 - \sum_{d_{1m}=1}^{d_{c1,m}} \mu_{[d_{1m}]}$.

In the following, we consider the code ensembles of the overall graph for s_m. For the NC scheme $\mathbb{C}_\oplus$, the relay transmits the network coded parity check digits to the destination within the total rate $R^{1,\text{nc}} = \sum_{m=1}^{M} R_m^{1,\text{nc}}$. There are $nR_m^{1,\text{nc}}$ effective digits allocated to s_m. According to *Theorem 2*, we can determine the value of $nR_m^{1,\text{nc}}$ and then decompose the overall graph in Fig. 6 into M sub-graphs. The m-th sub-graph for s_m contains the edge type $\mathcal{E}_{1m}$ in its lower sub-graph and the edge type $\mathcal{E}_{2m}$ in its upper sub-graph. Therefore, the polynomials of the m-th sub-graph are given by

$$\begin{aligned} v_m(\mathbf{r},\mathbf{x}) &= r_1 \sum_{d_{1m}=1}^{d_{v1,m}} \sum_{d_{2m}=0}^{d_{v2,m}} v_{[0,1],[d_{1m},d_{2m}]} x_{1m}^{d_{1m}} x_{2m}^{d_{2m}}, \\ \mu_m(\mathbf{x}) &= \sum_{d_{1m}=1}^{d_{c1,m}} \mu_{[d_{1m},0]} x_{1m}^{d_{1m}} + \sum_{d_{2m}=1}^{d_{c2,m}} \mu_{[0,d_{2m}]} x_{2m}^{d_{2m}}. \end{aligned} \tag{6}$$

Vector $\mathbf{b} = [0,1]$ of (6) remains similar to the ensemble of the m-th lower graph, which means that for the m-th sub-graph ensemble, all the variable nodes associated with the digits of s_m are transmitted through the $s_m \to d$ channel ($b_1 = 1$) at the rate R_m^-, and there are no punctured variables ($b_0 = 0$). Vector $[d_{1m}, d_{2m}]$ in (6) means that there are two edge types connected to a variable node in the m-th sub-graph, with d_{1m} and d_{2m} denoting the variable node degree of the two edge types $\mathcal{E}_{1m}$ and $\mathcal{E}_{2m}$, respectively. Vector $[d_{1m}, 0]$ means that there are only one edge type, *i.e.* $\mathcal{E}_{1m}$, connected to a check node in the m-th lower sub-graph, with d_{1m} denoting the check node degree of the edge type $\mathcal{E}_{1m}$. Vector $[0, d_{2m}]$ means that there are only one edge type, *i.e.* $\mathcal{E}_{2m}$, connected to a check node in the m-th upper sub-graph, with d_{2m} denoting the check node degree of the edge type $\mathcal{E}_{2m}$. The maximum edge numbers of $\mathcal{E}_{km}$, $(k = 1, 2)$ connected to a variable node and a check node are $d_{vk,m}$ and $d_{ck,m}$, respectively.

For the upper graph in Fig. 6, its ensemble is determined by the NC scheme $\mathbb{C}_\oplus$ at r. Here, we introduce the polynomial associated to the check nodes in the upper graph from the overall graph point of view, that is,

$$\mu(\mathbf{x}) = \sum_{d_{21}=0}^{d_{c2,1}} \cdots \sum_{d_{2M}=0}^{d_{c_2,M}} \mu_{[d_{21},\cdots,d_{2M}]} x_{21}^{d_{21}} \cdots x_{2M}^{d_{2M}}, \tag{7}$$

where vector $\mathbf{d} = [d_{21}, \cdots, d_{2M}]$ represents M edge types connected to the check nodes in the upper graph. We denote the numbers d_{21}, $\cdots$, d_{2M} as the edge numbers of $\mathcal{E}_{21}$, $\cdots$, $\mathcal{E}_{2M}$ that are connected to a check node in the upper graph, respectively. The coefficient $\mu_{[d_{21},\cdots,d_{2M}]}$ is uniquely determined by $\mathbb{C}_\oplus$. The relationship between $\mu_{[d_{21},\cdots,d_{2M}]}$ in (7) and $\mu_{[0,d_{2m}]}$ for the m-th sub-graph in (6) is

$$\begin{aligned} \mu_{[0,d_{2m}]} &= \sum_{\sim d_{2m}} \mu_{[d_{21},\cdots,d_{2M}]}, \quad \text{where} \\ \sum_{\sim d_{2m}} &= \sum_{d_{21}=0}^{d_{c2,1}} \cdots \sum_{d_{2(m-1)}=0}^{d_{c_2,m-1}} \sum_{d_{2(m+1)}=0}^{d_{c_2,m+1}} \cdots \sum_{d_{2M}=0}^{d_{c_2,M}}. \end{aligned} \tag{8}$$

Based on the polynomial of (7), we have the overall code rate from the relay to the destination as $R^{1,\text{nc}} = \sum_{d_{2m}=0}^{d_{c2,m}} \sum_{\sim d_{2m}} \mu_{[d_{21},\cdots,d_{2M}]}$. In the next step, we determine $R_m^{1,\text{nc}}$ for all m. Since each check node in the upper graph is shared by multiple sources, the value of $n\sum_{d_{2m}=1}^{d_{c2,m}} \mu_{[0,d_{2m}]}$ is the number of check nodes that have at least one edge belonging to type $\mathcal{E}_{2m}$. Therefore, we have the following inequality as $R_m^{1,\text{nc}} \le \sum_{d_{2m}=1}^{d_{c2,m}} \sum_{\sim d_{2m}} \mu_{[d_{21},\cdots,d_{2M}]}$. Recall that we have presented how to determine the effective parity check nodes for a network coding scheme $\mathbb{C}_\oplus$ in *Theorem 2*. Since we consider the successive decoding scheme at the destination, that is, the parity check digits are firstly decoded,

we can calculate $nR_m^{1,\mathrm{nc}}$ according to *Theorem 2* as

$$R_m^{1,\mathrm{nc}} = \sum_{d_{2m}=1}^{d_{c2,m}} \sum_{\sim d_{2m}} \frac{\mu_{[d_{21},\cdots,d_{2M}]} d_{2m}}{\sum_{l=1}^{M} d_{2l}}. \quad (9)$$

As mentioned in Section II, the network coding scheme $\mathbb{C}_{\oplus}$ should be designed to satisfy the achievable rate as given by (5). In order to clarify the presentation, we assume $R_m^{+} = R_m^{1,\mathrm{nc}} + R_m^{-}$ for all the M sources. At the destination, the code rate of s_m than can be successfully decoded is

$$\begin{aligned} R_m^{-} &= R_m^{+} - R_m^{1,\mathrm{nc}} \\ &= 1 - \sum_{d_{1m}=1}^{d_{c1,m}} \mu_{[d_{1m},0]} - \sum_{d_{2m}=1}^{d_{c2,m}} \sum_{\sim d_{2m}} \frac{\mu_{[d_{21},\cdots,d_{2M}]} d_{2m}}{\sum_{l=1}^{M} d_{2l}}. \end{aligned} \quad (10)$$

In addition, there are some other constraints that should be satisfied by the code. Firstly, there are degree constraints between the variable nodes and the check nodes for the m-th lower graph and the m-th sub-graph, respectively. That is, the total edges connected to the variable nodes are equal to the total edges connected to the check nodes. Therefore, we have $\sum_{d_{1m}=1}^{d_{c1,m}} \mu_{[d_{1m}]} d_{1m} = \sum_{d_{1m}=1}^{d_{v1,m}} v_{[0,1],[d_{1m}]} d_{1m}$ and $\sum_{d_{2m}=1}^{d_{c2,m}} \mu_{[0,d_{2m}]} d_{2m} = \sum_{d_{1m}=1}^{d_{v1,m}} \sum_{d_{2m}=0}^{d_{v2,m}} v_{[0,1],[d_{1m},d_{2m}]} d_{2m}$. The other constraints are the relationship between the m-th lower graph and the m-th sub-graph, *i.e.* $\mu_{[d_{1m}]} = \mu_{[d_{1m},0]}$ and $v_{[0,1],[d_{1m}]} = \sum_{d_{2,m=0}}^{d_{v2,m}} v_{[0,1],[d_{1m},d_{2m}]}$.

Here, we define some parameters, which will be used in the EXIT analysis in the next section. Firstly, we define $\lambda_{[d_{1m},d_{2m}]}^{km}$, $k = 1, 2$, as the percentage of the edges with the type $\mathcal{E}_{km}$, which are connected to the variable nodes with degree vector $[d_{1m}, d_{2m}]$. Then we have

$$\lambda_{[d_{1m},d_{2m}]}^{km} = \frac{v_{[0,1],[d_{1m},d_{2m}]} d_{km}}{\sum_{d_{1l}=1}^{d_{v1,m}} \sum_{d_{2l}=0}^{d_{v2,m}} v_{[0,1],[d_{1l},d_{2l}]} d_{kl}}. \quad (11)$$

We define $\lambda_{[d_{1m},d_{2m}]}^{m}$ as the percentage of the edges connected to the variable nodes with degree vector $[d_{1m}, d_{2m}]$. These latter edges come from either type $\mathcal{E}_{1m}$ or type $\mathcal{E}_{2m}$. Then we have

$$\lambda_{[d_{1m},d_{2m}]}^{m} = \frac{v_{[0,1],[d_{1m},d_{2m}]} (d_{1m} + d_{2m})}{\sum_{d_{1l}=1}^{d_{v1,m}} \sum_{d_{2l}=0}^{d_{v2,m}} v_{[0,1],[d_{1l},d_{2l}]} (d_{1l} + d_{2l})}. \quad (12)$$

We also define $\rho_{[d_{1m}]}^{1,m}$ as the percentage of the edges in the type $\mathcal{E}_{1m}$, which are connected to the check nodes in the m-th lower sub-graph with degree vector $[d_{1m}]$, that is,

$$\rho_{[d_{1m}]}^{1m} = \frac{\mu_{[d_{1m}]} d_{1m}}{\sum_{d_{1l}=1}^{d_{c1,m}} \mu_{[d_{1l}]} d_{1l}}. \quad (13)$$

Finally, we define $\rho_{[d_{21},\cdots,d_{2M}]}^{2m}$ as the percentage of the edges of the type $\mathcal{E}_{2m}$, which are connected to the check nodes in the upper graph with degree vector $[d_{21}, \cdots, d_{2M}]$, that is,

$$\rho_{[d_{21},\cdots,d_{2M}]}^{2m} = \frac{\mu_{[d_{21},\cdots,d_{2M}]} d_{2m}}{\sum_{d_{2l}=0}^{d_{c2,m}} \mu_{[0,d_{2l}]} d_{2l}}. \quad (14)$$

Since the blocks of all the sources are connected by the NC scheme, we can view these blocks as a super block. In the next section, we will optimize the NC scheme for the system.

V. EXIT Analysis and Codes Profile Optimization

For turbo and LDPC codes, EXIT charts can characterize the extrinsic mutual information (EMI) between the input and the output of the component decoders. EXIT charts can also facilitate the analysis of the coding schemes and aid in the construction of optimum codes ensembles. In this section, we exploit the EXIT functions [21–23] to design the optimal NCMET-LDPC codes for the $M - 1 - 1$ system.

We notice that in the conventional EXIT chart analysis, the calculated EMI values at the check nodes in [22] are always larger than the exact values [25]. This is because of the assumption that the EMI produced by the check nodes follows a Gaussian distribution. In [26, 27], the authors give a more accurate method of the calculation of the EMI produced by the check nodes. Utilizing this method, we propose a new approach to the EXIT analysis for the NCMET-LDPC codes, and then present how to optimize the code profiles based on EXIT charts.

A. EMI Propagation Model

Since the codeword digits of different sources experience different channel conditions, we average the EMI in each edge type when computing EMI. We denote the variable nodes set associated with the codeword digits of s_m as V_m, the check nodes set associated with the parity check digits of s_m in the m-th lower graph as C_{1m}, and the shared check nodes set associated with the network coded parity check digits of the relay in the upper graph as C_2. The mutual information of the $s_m \to d$ channel is denotes as I_{ch}^m. Since V_m is connected to two edge types, *i.e.* $\mathcal{E}_{1m}$ and $\mathcal{E}_{2m}$, we define four kinds of EMI as follows [23].

1. I_{Ev}^{1m}: The EMI between the message sent from V_m to C_{1m} and the associated codeword digit, on each edge of the type $\mathcal{E}_{1m}$ connecting V_m to C_{1m};
2. I_{Ev}^{2m}: The EMI between the message sent from V_m to C_2 and the associated codeword digit, on each edge of the type $\mathcal{E}_{2m}$ connecting V_m to C_2;
3. I_{Ec}^{1m}: The EMI between the message sent from C_{1m} to V_m and the associated codeword digit, on each edge of the edge type $\mathcal{E}_{1m}$ connecting C_{1m} to V_m;
4. I_{Ec}^{2m}: The EMI between the message sent from C_2 to V_m and the associated codeword digit, on each edge of the edge type $\mathcal{E}_{2m}$ connecting C_2 to V_m.

Also note that the EMI on an edge connecting V_m to C_{1m} (or C_2), at the output of the variable node, is the a-priori mutual information (AMI) for C_{1m} (or C_2), *i.e.* $I_{Ev}^{1m} = I_{Ac}^{1m}$ (or $I_{Ev}^{2m} = I_{Ac}^{2m}$). Similarly, the EMI on an edge connecting C_{1m} (or C_2) to V_m, at the output of the check node, is the AMI for V_m, *i.e.* $I_{Ec}^{1m} = I_{Av}^{1m}$ (or $I_{Ec}^{2m} = I_{Av}^{2m}$).

B. EXIT Analysis for the NCMET-LDPC codes

The EXIT function for variable nodes and check nodes in an AWGN channel was introduced in [22]. For the signals transmitted by s_m, we define $(1/\sigma_m)^2$ as the received signal-to-noise ratio (SNR) at the destination. For the log-likelihood ratio (LLR) obtained at the output of the $s_m \to d$ channel, we denote its variance as $(\sigma_{ch}^m)^2$ [21]. Therefore, we have the

relationship $\sigma_{ch}^m = 2/\sigma_m$. Since each source transmits BPSK symbols, we use $J(\sigma_{ch}^m)$ to represent the mutual information of a binary input additive Gaussian noise channel, which is given by [21]

$$J(\sigma_{ch}^m) = 1 - \int_{-\infty}^{+\infty} \frac{e^{-\left(\xi-(\sigma_{ch}^m)^2/2\right)^2/2(\sigma_{ch}^m)^2}}{\sqrt{2\pi}\sigma_{ch}^m} \cdot \log_2(1+e^{-\xi}) \mathrm{d}\xi \tag{15}$$

where the integral variable ξ represents the LLR value of the channel. We now construct the following iterative process for EMI.

1. Initialization

We initialize that $I_{ch}^m = J(\sigma_{ch}^m)$, for $m = 1, \cdots, M$.

2. Variable nodes to check nodes update

For $m = 1, \cdots, M$, $k = 1, 2$, and $\bar{k} = 3 - k$, we have

$$I_{Ev}^{km} = \sum_{d_{km}=1}^{d_{vk,m}} \sum_{d_{\bar{k}m}=0}^{d_{v\bar{k},m}} J\left(\sqrt{\varphi_V^{km}}\right) \lambda_{[d_{km},d_{\bar{k}m}]}^{km}, \tag{16}$$

where $\varphi_V^{km} = (d_{km} - 1)\left(J^{-1}\left(I_{Av}^{km}\right)\right)^2 + d_{\bar{k}m}\left(J^{-1}\left(I_{Av}^{\bar{k}m}\right)\right)^2 + \left(J^{-1}\left(I_{ch}^m\right)\right)^2$.

3. Check nodes to variable nodes update

To obtain the accurate EMI value at the check nodes, we follow the method in [26, 27]. According to [26, 27], we define the function $F_j(\sigma)$ as follows.

$$F_j(\sigma) = \int_{-1}^{+1} \frac{2\zeta^{2j}}{(1-\zeta^2)\sqrt{2\pi}\sigma} e^{-\frac{\left(\ln\frac{1+\zeta}{1-\zeta} - \frac{\sigma^2}{2}\right)^2}{2\sigma^2}} \mathrm{d}\zeta, \tag{17}$$

where the integral variable ζ represents the "soft bit" message corresponding to the LLR message ξ_ζ by $\zeta = \tanh((\xi_\zeta)/2)$. Then the EMI on an edge type $\mathcal{E}_{1m}$ connecting C_{1m} to V_m, at the output of the check node is

$$I_{Ec}^{1m} = \frac{1}{\ln 2} \sum_{d_{1m}=1}^{d_{c1,m}} \sum_{j=1}^{\infty} \frac{\left(F_j\left(J^{-1}(I_{Ac}^{1m})\right)\right)^{d_{1m}-1}}{2j(2j-1)} \rho_{[d_{1m}]}^{1m}. \tag{18}$$

The EMI on an edge type $\mathcal{E}_{2m}$ connecting C_2 to V_m at the output of the check node is more complicated since more than one source participates in the generation of C_2. We have

$$I_{Ec}^{2m} = \frac{1}{\ln 2} \sum_{d_{2m}=1}^{d_{c2,m}} \sum_{\sim d_{2m}} \sum_{j=1}^{\infty} \frac{\rho_{[d_{21},\cdots,d_{2M}]}^{2m}}{2j(2j-1)} \left(F_j\left(J^{-1}(I_{Ac}^{2m})\right)\right)^{d_{2m}-1} \prod_{\substack{m'=1 \\ m'\neq m}}^{M} \left(F_j\left(J^{-1}(I_{Ac}^{2m'})\right)\right)^{d_{2m'}}. \tag{19}$$

After the update from check nodes to variable nodes, go to step **2** and begin the next round iteration. In each iteration process, we make $I_{Av}^{km} = I_{Ec}^{km}$ and $I_{Ac}^{km} = I_{Ev}^{km}$ for $k = 1, 2$.

4. Output and decision

At the end of the iteration, we get the output of the mutual information between the V_m and the associated codeword digits denoted as I_m. For $m = 1, \cdots, M$, we have

$$I_V^m = \sum_{d_{1m}=1}^{d_{v1,m}} \sum_{d_{2m}=0}^{d_{v2,m}} \lambda_{[d_{1m},d_{2m}]}^m J\left(\sqrt{\varphi_V^m}\right), \tag{20}$$

where $\varphi_V^m = d_{1m}\left(J^{-1}\left(I_{Av}^{1m}\right)\right)^2 + d_{2m}\left(J^{-1}\left(I_{Av}^{2m}\right)\right)^2 + \left(J^{-1}\left(I_{ch}^m\right)\right)^2$. We make the prediction of a successful decoding based on whether I_V^m approaches to 1, $m = 1, \cdots, M$.

C. Code Design and Optimization

In the code design for the proposed NCMET-LDPC codes, we firstly fix the lower graph codes of all sources by choosing the optimal point-to-point LDPC code to approach the rate R_m^+. Then we optimize the overall graph to approach the achievable rate of the whole system. The code optimization involves finding the optimal degree distributions of the variable nodes associated with the digits of each source, *i.e.* $v_{[0,1],[d_{1m},d_{2m}]}$ for s_m, and the optimal check node degree distribution $\mu_{[d_{21},\cdots,d_{2M}]}$. The optimization problem is to maximize the system threshold, which is explained as follows. Since the mutual information of the $s_m \to d$ channel is $J(\frac{2}{\sigma_m})$ and all the sources have the same block length, we compute the system mutual information as the average of the channel mutual information of all the sources. We can therefore write the system threshold as

$$\sigma_{sys} = \frac{2}{J^{-1}\left(\frac{1}{M}\sum_{m=1}^{M} J\left(\frac{2}{\sigma_m}\right)\right)}. \tag{21}$$

Then the optimization problem is formulated as maximizing σ_{sys}, subject to $I(m) \to 1$, for $m = 1, \cdots, M$.

VI. Simulations

We compare our code designs for NC with known SP schemes. We ensure that in both the NC and the SP schemes the sources' blocks (codewords) all have the same length. We also ensure that the relay (in both schemes) utilizes the same number of additional bits. Finally, we ensure the achievable rates for the two schemes are the same. These three conditions in turn, ensure that the number of bits being used at the receiver is the same for both the NC and SP schemes - thus allowing a direct and fair comparison. The detailed comparisons we investigate are for a $2-1-1$ relay system and a $3-1-1$ relay system, where the sources' and the relay's block lengths are set to $n = 10^4$. All signals are assumed to be BPSK modulated.

For each single-source relay system, we choose one of the following three rate groups (RGs).

RG 1: $R_1^+ = 0.7$, $R_1^- = 0.5$, and $R_1^1 = 0.2$.

RG 2: $R_2^+ = 0.58$, $R_2^- = 0.38$, and $R_2^1 = 0.2$.

RG 3: $R_3^+ = 0.7$, $R_3^- = 0.38$, and $R_3^1 = 0.32$.

We choose the three rate groups so that (a) RG 1 and RG 2 have the same R^1; (2) RG 1 and RG 3 have the same R^+; (3) RG 2 and RG 3 have the same R^-. There are three combinations of these RGs for the $2-1-1$ two-source relay system. We will consider the following three cases:

Case 1: The two $1-1-1$ systems have the RG 1 and RG 2, respectively.

Case 2: The two $1-1-1$ systems have the RG 1 and RG 3, respectively.

Case 3: The two $1-1-1$ systems have the RG 3 and RG 2, respectively.

For the $3-1-1$ system, we will consider the following case:

TABLE I
THE NODE DISTRIBUTIONS OF THE NCMET-LDPC CODE AND THE BMET-LDPC CODE FOR CASE 1.

NCMET-LDPC code (CODE-D):NC						**BMET-LDPC code (CODE-AB):SP**					
Rate Group 1			**Rate Group** 2			**Rate Group** 1			**Rate Group** 2		
Variable Node Distribution						**Variable Node Distribution**					
$v_{[0,1][d_{11},d_{21}]}$	$\mathcal{E}_{11}$	$\mathcal{E}_{21}$	$v_{[0,1][d_{12},d_{22}]}$	$\mathcal{E}_{12}$	$\mathcal{E}_{22}$	$v_{[0,1][d_{11},d_{21}]}$	$\mathcal{E}_{11}$	$\mathcal{E}_{21}$	$v_{[0,1][d_{12},d_{22}]}$	$\mathcal{E}_{12}$	$\mathcal{E}_{22}$
0.244225	2	0	0.3289203	2	0	0.247137	2	0	0.343893	2	0
0.1531552	2	1	0.0772109	2	1	0.143731	2	1	0.115366	2	1
0.0209422	2	7	0.0531292	2	2	0.027432	2	6	0.17937	3	0
0.1930021	3	0	0.145309	3	0	0.191186	3	0	0.13334	3	1
0.138759	3	3	0.0149215	3	1	0.135883	3	1	0.0158	6	3
0.058304	6	0	0.123802	3	2	0.004730	3	3	0.02901	6	11
0.0109062	6	7	0.0286741	3	14	0.025454	6	3	0.1223	7	2
0.000131148	6	21	0.0346943	6	0	0.043946	6	9	0.0314072	20	1
0.05680712	7	0	0.0101216	6	2	0.071606	7	1	0.029511	20	4
0.047728	7	2	0.092595	7	0	0.032894	7	2			
0.0556525	20	3	0.0297043	7	7	0.039999	20	2			
0.0203505	20	7	0.0165257	20	0	0.036001	20	7			
			0.00437642	20	1						
			0.0400163	20	3						
Check Node Distribution in Lower Graph						**Check Node Distribution in Lower Graph**					
$\mu_{[d_{11},0]}$		$\mathcal{E}_{11}$	$\mu_{[d_{12},0]}$		$\mathcal{E}_{12}$	$\mu_{[d_{11},0]}$		$\mathcal{E}_{11}$	$\mu_{[d_{12},0]}$		$\mathcal{E}_{12}$
0.3		15	0.42		10	0.3		15	0.42		10
Check Node Distribution in Upper Graph						**Check Node Distribution in Upper Graph**					
$\mu_{[d_{21},d_{22}]} \times \frac{R_1^1}{R_1^1+R_2^1}$		$\mathcal{E}_{21}$	$\mu_{[d_{21},d_{22}]} \times \frac{R_2^1}{R_1^1+R_2^1}$		$\mathcal{E}_{22}$	$\mu_{[0,d_{21}]}$		$\mathcal{E}_{21}$	$\mu_{[0,d_{22}]}$		$\mathcal{E}_{22}$
0.2		3	0.2		3	0.082626		6	0.1907		5
						0.117374		7	0.0093		6

TABLE II
THE NODE DISTRIBUTIONS OF THE NCMET-LDPC CODE AND THE BMET-LDPC CODE FOR CASE 2.

NCMET-LDPC code (CODE-E):NC						**BMET-LDPC code (CODE-AC):SP**					
Rate Group 1			**Rate Group** 3			**Rate Group** 1			**Rate Group** 3		
Variable Node Distribution						**Variable Node Distribution**					
$v_{[0,1][d_{11},d_{21}]}$	$\mathcal{E}_{11}$	$\mathcal{E}_{21}$	$v_{[0,1][d_{12},d_{22}]}$	$\mathcal{E}_{12}$	$\mathcal{E}_{22}$	$v_{[0,1][d_{11},d_{21}]}$	$\mathcal{E}_{11}$	$\mathcal{E}_{21}$	$v_{[0,1][d_{12},d_{22}]}$	$\mathcal{E}_{12}$	$\mathcal{E}_{22}$
0.265783	2	0	0.1910361	2	0	0.247137	2	0	0.19731	2	0
0.111465	2	1	0.0703665	2	1	0.143731	2	1	0.058866	2	1
0.0410082	2	2	0.15692	2	2	0.027432	2	6	0.15335	2	3
0.00006559	2	20	0.13737	3	0	0.191186	3	0	0.0087948	2	20
0.1611	3	0	0.156199	3	1	0.135883	3	1	0.16175	3	0
0.0837898	3	1	0.00488247	3	7	0.004730	3	3	0.066858	3	1
0.0758774	3	6	0.0333089	3	14	0.025454	6	3	0.10315	3	3
0.0109938	3	7	0.0626549	6	0	0.043946	6	9	0.069378	6	0
0.0207645	6	0	0.00672323	6	7	0.071606	7	1	0.069062	7	1
0.04861368	6	2	0.0896714	7	3	0.032894	7	2	0.035473	7	4
0.0570473	7	0	0.0148637	7	7	0.039999	20	2	0.039814	20	4
0.0436473	7	3	0.01462617	20	2	0.036001	20	7	0.036189	20	11
0.0038405	7	6	0.0613769	20	7						
0.0157611	20	0									
0.0592666	20	2									
0.00097531	20	20									
Check Node Distribution in Lower Graph						**Check Node Distribution in Lower Graph**					
$\mu_{[d_{11},0]}$		$\mathcal{E}_{11}$	$\mu_{[d_{12},0]}$		$\mathcal{E}_{12}$	$\mu_{[d_{11},0]}$		$\mathcal{E}_{11}$	$\mu_{[d_{12},0]}$		$\mathcal{E}_{12}$
0.3		15	0.3		15	0.3		15	0.3		15
Check Node Distribution in Upper Graph						**Check Node Distribution in Upper Graph**					
$\mu_{[d_{21},d_{22}]} \times \frac{R_1^1}{R_1^1+R_2^1}$		$\mathcal{E}_{21}$	$\mu_{[d_{21},d_{22}]} \times \frac{R_2^1}{R_1^1+R_2^1}$		$\mathcal{E}_{22}$	$\mu_{[0,d_{21}]}$		$\mathcal{E}_{21}$	$\mu_{[0,d_{22}]}$		$\mathcal{E}_{22}$
0.1200182533		2	0.2400365067		4	0.082626		6	0.080591		5
0.07997262		3	0.07997262		3	0.117374		7	0.23941		6

Case 4: The three $1-1-1$ systems have the RG 1, RG 2 and RG 3, respectively.

Note that, in Case 1, the r_1-to-d channel and the r_2-to-d channel have the same rate, *i.e.* $R_1^1 = R_2^1 = 0.2$. In Case 2, the s_1-to-r_1 channel and the s_2-to-r_2 channel have the same rate, *i.e.* $R_1^+ = R_3^+ = 0.7$. In Case 3, the s_1-to-d channel and the s_2-to-d channel have the same rate, *i.e.* $R_3^- = R_2^- = 0.38$. For each case with NC scheme, we design the NCMET-LDPC codes with corresponding RGs. For comparison purpose, we design the bilayer multi-edge type LDPC (BMET-LDPC) codes [7] for SP with corresponding RGs. In the simulation, we will compare NCMET-LDPC codes with BMET-LDPC codes.

More specifically, for the NC scheme in the $2-1-1$ system, we first determine the degree distributions of $\mathcal{E}_{11}$ and $\mathcal{E}_{12}$ in the lower graphs for s_1 and s_2 to approach the rates of the source-

to-destination channels, R_1^+ and R_2^+, respectively. The degree distributions are designed similar to single link LDPC codes and can be directly obtained from [28]. Then we optimize the NCMET-LDPC codes by searching the distributions of $\mathcal{E}_{21}$ and $\mathcal{E}_{22}$, and the corresponding $v_{[0,1][d_{1,1},d_{2,1}]}$, $v_{[0,1][d_{1,2},d_{2,2}]}$ and $\mu_{[0,d_{2,1},d_{2,2}]}$. To compare with the code design in the SP scheme, we directly apply the BMET-LDPC codes to each $1-1-1$ single-source relay system. We design three BMET-LDPC codes, named CODE-A, CODE-B, and CODE-C for the $1-1-1$ single-source relay system with the three RGs, respectively, based on the method in [7]. Then for each case with the SP scheme, we directly employ the BMET-LDPC codes of the corresponding RGs. We design the codes for the $3-1-1$ system by following the similar way.

A. Codes for Case 1

By the searching criterion in the previous section, we obtain an NEMET-LDPC code for Case 1. The distributions of the variable nodes in the code, *i.e.* $v_{[0,1][d_{1,1},d_{2,1}]}$, $v_{[0,1][d_{1,2},d_{2,2}]}$, and the corresponding degrees are shown in Table I. The distribution of the check nodes in the upper graph is $\mu_{[d_{21},d_{22}]} = R_1^1 + R_2^1 = 0.4$. Each check node in the upper graph has the degree 6, among which, 3 edges are allocated to s_1 and the other 3 edges are allocated to s_2. This is due to the fact that $R_1^1 = R_2^1 = 0.2$. Note that the gap between the Shannon limits for the two rates, *i.e.* $R_1^- = 0.5$ and $R_2^- = 0.38$ is about 1.65 dB. Therefore, during the code search, we set the gap between the two thresholds σ_1 and σ_2 according to their Shannon limit gap, and we obtain the two thresholds as $\sigma_1 = 0.9692$ and $\sigma_2 = 1.1519$.

We refer to the NCMET-LDPC code for Case 1 in the Table I as CODE-D. For the $2-1-1$ system with the SP method, the BMET-LDPC code for this case with SP are also shown in the Table I, which is referred to as CODE-AB. Note that we do not need to jointly search CODE-AB for RG1 and RG2 in the $2-1-1$ system. Since we already have CODE-A and CODE-B for RG1 and RG2, respectively. CODE-AB is directly obtained by combining CODE-A and CODE-B.

B. Codes for Case 2

We obtain an NCMET-LDPC code for Case 2 shown in Table II. The distribution of check nodes in the upper graph is $\mu_{[d_{21},d_{22}]} = R_1^1 + R_3^1 = 0.52$. Each check node in the upper graph has the degree 6. However, 69.2413% of these check nodes have 2 edges of type $\mathcal{E}_{21}$ and 4 edges of type $\mathcal{E}_{23}$, and 30.7587% of these check nodes have 3 edges of type $\mathcal{E}_{21}$ and 3 edges of type $\mathcal{E}_{23}$. Also, according to the gap between the Shannon limits for the two rates, *i.e.* $R_1^- = 0.5$ and $R_3^- = 0.38$, the two thresholds that we obtain are $\sigma_1 = 0.9705$ and $\sigma_3 = 1.1531$, respectively. We refer to the NCMET-LDPC code in Table II as CODE-E, which is jointly searched for both RG1 and RG3. For comparison, the BMET-LDPC code for Case 2 with SP are also shown in the Table II. It is referred to as CODE-AC, which is the combination of CODE-A and CODE-C.

TABLE III
THE NODE DISTRIBUTION OF THE NCMET-LDPC CODE FOR CASE 3.

NCMET-LDPC code (CODE-F):NC					
Rate Group 3			**Rate Group** 2		
Variable Node Distribution					
$v_{[0,1][d_{11},d_{21}]}$	$\mathcal{E}_{11}$	$\mathcal{E}_{21}$	$v_{[0,1][d_{12},d_{22}]}$	$\mathcal{E}_{12}$	$\mathcal{E}_{22}$
0.1318982	2	0	0.3224905	2	0
0.1692057	2	1	0.106892	2	1
0.117219	2	6	0.0298767	2	3
0.2634388	3	0	0.1701424	3	0
0.0683222	3	7	0.123784	3	1
0.0585838	6	1	0.0187803	3	20
0.00878041	6	3	0.00912155	6	0
0.00201396	6	20	0.0356944	6	3
0.0414464	7	1	0.0557519	7	0
0.0569312	7	3	0.050545	7	2
0.00615748	7	20	0.0160023	7	7
0.0154696	20	0	0.0137815	20	0
0.0364705	20	1	0.0292194	20	2
0.0240629	20	3	0.0179176	20	7
Check Node Distribution in Lower Graph					
$\mu_{[d_{11},0]}$	$\mathcal{E}_{11}$		$\mu_{[d_{12},0]}$		$\mathcal{E}_{12}$
0.3	15		0.42		10
Check Node Distribution in Upper Graph					
$\mu_{[d_{21},d_{22}]} \times \frac{R_1^1}{R_1^1+R_2^1}$	$\mathcal{E}_{21}$		$\mu_{[d_{21},d_{22}]} \times \frac{R_2^1}{R_1^1+R_2^1}$		$\mathcal{E}_{22}$
0.2400202133	4		0.1200101067		2
0.07998484	3		0.07998484		3

C. Codes for Case 3

We obtain an NCMET-LDPC code for Case 3 shown in Table III. The distribution of check nodes in the upper graph is $\mu_{[d_{23},d_{22}]} = R_3^1 + R_2^1 = 0.52$. Each check node in the upper graph has the degree 6. However, 69.2366% of these check nodes have 2 edges of type $\mathcal{E}_{23}$ and 4 edges of type $\mathcal{E}_{22}$, and 30.7634% of these check nodes have 3 edges of type $\mathcal{E}_{23}$ and 3 edges of type $\mathcal{E}_{22}$. Since the two RGs have the same s-to-d rate, *i.e.* $R_3^- = R_2^- = 0.38$, we obtain the same threshold as $\sigma_3 = \sigma_2 = 1.1564$, respectively. We refer the NCMET-LDPC code in Table III as CODE-F, which is jointly searched for both RG3 and RG2. We also obtain the BMET-LDPC code referred to as CODE-CB for Case 3 with SP, which is the combination of CODE-C and CODE-B.

D. Codes for Case 4

We obtain an NCMET-LDPC code for Case 4 shown in Table IV. The distribution of check nodes in the upper graph is $\mu_{[d_{21},d_{22},d_{23}]} = R_1^1 + R_2^1 + R_3^1 = 0.72$. Each check node in the upper graph has the degree 6. In the upper graph, 33.3% of these check nodes have 2 edges of type $\mathcal{E}_{21}$, 2 edges of type $\mathcal{E}_{22}$ and 2 edges of type $\mathcal{E}_{23}$, 33.3% of these check nodes have 1 edges of type $\mathcal{E}_{21}$, 2 edges of type $\mathcal{E}_{22}$ and 3 edges of type $\mathcal{E}_{23}$, and 33.3% of these check nodes have 2 edges of type $\mathcal{E}_{21}$, 1 edges of type $\mathcal{E}_{22}$ and 3 edges of type $\mathcal{E}_{23}$. We obtain the thresholds for the three RGs as $\sigma_1 = 0.969, \sigma_2 = 1.1525$, and $\sigma_3 = 1.1515$ respectively. We refer the NCMET-LDPC code in Table IV as CODE-G, which is jointly searched for all three RGs. We also obtain the BMET-LDPC code referred to as CODE-ABC for Case 4 with SP, which is the combination of CODE-A, CODE-B and CODE-C.

TABLE IV
THE NODE DISTRIBUTION OF THE NCMET-LDPC CODE FOR CASE 4.

NCMET-LDPC code (CODE-G):NC								
Rate Group 1			**Rate Group** 2			**Rate Group** 3		
Variable Node Distribution								
$v_{[0,1][d_{11},d_{21}]}$	$\mathcal{E}_{11}$	$\mathcal{E}_{21}$	$v_{[0,1][d_{12},d_{22}]}$	$\mathcal{E}_{12}$	$\mathcal{E}_{22}$	$v_{[0,1][d_{13},d_{23}]}$	$\mathcal{E}_{13}$	$\mathcal{E}_{23}$
0.2635483	2	0	0.270639	2	0	0.2155186	2	0
0.112911	2	1	0.117386	2	1	0.154023	2	2
0.0418626	2	7	0.0642334	2	3	0.0305867	2	3
0.149117	3	0	0.00700072	2	6	0.0181946	2	14
0.163466	3	1	0.2829063	3	0	0.0841675	3	0
0.007709	3	2	0.0298002	3	2	0.2475941	3	3
0.0114686	3	14	0.024855	6	7	0.047222	6	0
0.0338925	6	0	0.0199609	6	14	0.0219735	6	2
0.03548559	6	6	0.0463214	7	1	0.000182611	6	13
0.0373675	7	0	0.07597779	7	2	0.0956172	7	0
0.0626623	7	1	0.0331672	20	1	0.00891793	7	6
0.0045052	7	14	0.0210431	20	3	0.00510349	20	0
0.0180071	20	0	0.00670818	20	6	0.0585315	20	3
0.0579959	20	2				0.012368	20	20
Check Node Distribution in Lower Graph								
$\mu_{[d_{11},0]}$		$\mathcal{E}_{11}$	$\mu_{[d_{12},0]}$		$\mathcal{E}_{12}$	$\mu_{[d_{13},0]}$		$\mathcal{E}_{13}$
0.3		15	0.42		10	0.3		15
Check Node Distribution in Upper Graph								
$\mu_{[d_{21},d_{22},d_{23}]} \times \frac{R_1^1}{R_1^1+R_2^1+R_3^1}$		$\mathcal{E}_{21}$	$\mu_{[d_{21},d_{22},d_{23}]} \times \frac{R_2^1}{R_1^1+R_2^1+R_3^1}$		$\mathcal{E}_{22}$	$\mu_{[d_{21},d_{22},d_{23}]} \times \frac{R_3^1}{R_1^1+R_2^1+R_3^1}$		$\mathcal{E}_{23}$
0.08		2	0.08		2	0.08		2
0.04		1	0.08		2	0.12		3
0.08		2	0.04		1	0.12		3

E. BER curves

We investigate the bit error rate (BER) performance for various coding schemes. Note that the parity check digits transmitted by the relay are firstly decoded. Therefore, we do not need to consider the SNR in the r-to-d channels. The two SNRs of the sources at the destination are denoted as ρ_1 and ρ_2. The system SNR in the BER curves for the $2-1-1$ system is defined as $\rho_{sys} = \left[\frac{1}{2}J^{-1}(\frac{1}{2}(J(2\sqrt{\rho_1}) + J(2\sqrt{\rho_2}))\right]^2$. The system SNR for the $3-1-1$ system is defined as $\rho_{sys} = \left[\frac{1}{2}J^{-1}(\frac{1}{3}(J(2\sqrt{\rho_1}) + J(2\sqrt{\rho_2}) + J(2\sqrt{\rho_3}))\right]^2$.

Fig. 7 shows the BER curves of the designed NCMET-LDPC codes and BMET-LDPC codes for the $2-1-1$ relay system with various RGs. Note that the BER curves are presented for each source separately in CODE-D, CODE-E, and CODE-F. In Case 1, there are two RGs, *i.e.* RG1 and RG2. We compare the NCMET-LDPC code (CODE-D) with the BMET-LDPC codes (CODE-A and CODE-B) for the two RGs. For RG1, CODE-D is better than CODE-A by 0.23-dB at the BER of 10^{-4}. For RG2, CODE-D is better than CODE-B by 0.17-dB at the BER of 10^{-4}. In Case 2, there are two RGs, *i.e.* RG1 and RG3. We compare the NCMET-LDPC code (CODE-E) with the BMET-LDPC codes (CODE-A and CODE-C) for the two RGs. For RG1, CODE-E is better than CODE-A by 0.25-dB at the BER of 10^{-4}. For RG3, CODE-E is better than CODE-C by 0.18-dB at the BER of 10^{-4}. In Case 3, there are two RGs, *i.e.* RG3 and RG2. We compare the NCMET-LDPC code (CODE-F) with the BMET-LDPC codes (CODE-C and CODE-B) for the two RGs. For RG3, CODE-F is better than CODE-C by 0.3-dB at the BER of 10^{-4}. For RG2, CODE-F is better than CODE-B by 0.35-dB at the BER of 10^{-4}. We can see that NCMET-LDPC codes for all RGs are better than that of BMET-LDPC codes.

Note that the performance gain of the proposed NCMET-LDPC codes relative to BMET-LDPC codes is due to that (1) the network codes are optimized based on all the sources' codes to achieve higher threshold, and (2) the optimized network codes enable a jointly decoding among all the sources' codewords at the destination.

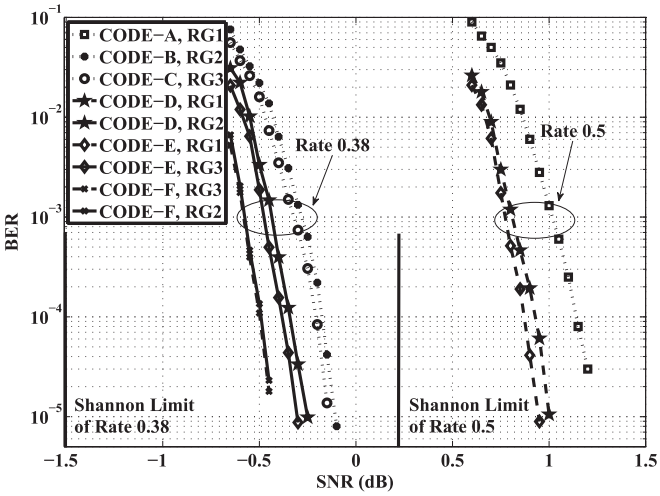

Fig. 7. BER curves of the designed NCMET-LDPC codes and BMET-LDPC codes for the three cases in the $2-1-1$ relay system. The BER curve for each RG is plotted. In Case 1, there are two RGs, *i.e.* RG1 and RG2. We compare the NCMET-LDPC code (CODE-D) with the BMET-LDPC codes (CODE-A and CODE-B) for the two RGs. The two thresholds of CODE-D for the two RGs are $\sigma_1 = 0.9692$ and $\sigma_2 = 1.1519$. In Case 2, there are two RGs, *i.e.* RG1 and RG3. We compare the NCMET-LDPC code (CODE-E) with the BMET-LDPC codes (CODE-A and CODE-C) for the two RGs. The two thresholds of CODE-E for the two RGs are $\sigma_1 = 0.9705$ and $\sigma_3 = 1.1531$. In Case 3, there are two RGs, *i.e.* RG3 and RG2. We compare the NCMET-LDPC code (CODE-F) with the BMET-LDPC codes (CODE-C and CODE-B) for the two RGs. The two thresholds of CODE-F for the two RGs are $\sigma_3 = \sigma_2 = 1.1564$.

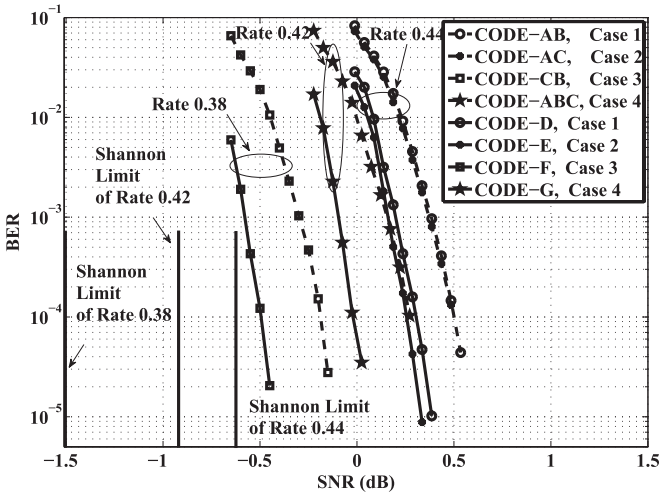

Fig. 8. BER curves of designed NCMET-LDPC codes and BMET-LDPC codes for all the cases from the whole system point of view. In Case 1, the system rate is $(R_1^- + R_2^-)/2 = 0.44$. The BER of CODE-AB for the system is calculated by averaging the BERs of CODE-A and CODE-B. We compare the NCMET-LDPC code (CODE-D) with the BMET-LDPC code (CODE-AB) for the Case 1. In Case 2, the system rate is $(R_1^- + R_3^-)/2 = 0.44$. We compare the NCMET-LDPC code (CODE-E) with the BMET-LDPC code (CODE-AC) for Case 2. In Case 3, the system rate is $(R_3^- + R_2^-)/2 = 0.38$. We compare the NCMET-LDPC code (CODE-F) with the BMET-LDPC code (CODE-CB) for Case 3. In Case 4, the system rate is $(R_1^- + R_2^- + R_3^-)/3 = 0.42$. We compare the NCMET-LDPC code (CODE-G) with the BMET-LDPC code (CODE-ABC) for Case 4.

Fig. 8 shows the BER curves of designed NCMET-LDPC codes and BMET-LDPC codes from the whole system point of view. The system rate in each case is calculated according to rates of the two RGs. Note that all the frames transmitted by the sources and the relay have the same length. In Case 1, the system rate is $(R_1^- + R_2^-)/2 = (0.5 + 0.38)/2 = 0.44$. The BER of CODE-AB for the system is calculated by averaging the BERs of CODE-A and CODE-B. Comparing the NCMET-LDPC code (CODE-D) with the BMET-LDPC code (CODE-AB) for the Case 1, we can see from Fig. 8 that CODE-D is better than CODE-AB by 0.23-dB at the BER of 10^{-4}. In Case 2, the system rate is $(R_1^- + R_3^-)/2 = (0.5 + 0.38)/2 = 0.44$. Comparing the NCMET-LDPC code (CODE-E) with the BMET-LDPC code (CODE-AC) for Case 2, from Fig. 8, CODE-E is better than CODE-AC by 0.24-dB at the BER of 10^{-4}. In Case 3, the system rate is $(R_3^- + R_2^-)/2 = (0.38 + 0.38)/2 = 0.38$. Comparing the NCMET-LDPC code (CODE-F) with the BMET-LDPC code (CODE-CB) for Case 3, from Fig. 8, CODE-F is better than CODE-CB by 0.32-dB at the BER of 10^{-4}. In Case 4, the system rate is $(R_1^- + R_2^- + R_3^-)/3 = (0.5 + 0.38 + 0.38)/3 = 0.42$. Comparing the NCMET-LDPC code (CODE-G) with the BMET-LDPC code (CODE-ABC) for Case 4, from Fig. 8, CODE-F is better than CODE-CB by 0.32-dB at 10^{-4}.

VII. Conclusion

In this work, we have explored new approaches to LDPC code design for a multi-source single-relay FDMA system, under the assumption of uniform phase-fading Gaussian channels. The key aspects of our study are the introduction of asymmetric channels for multiple sources, and the utilization of network coding at the relay. To assist with our designs, we proposed a *binary field rate splitting theorem* that was subsequently used to discover an appropriate NC scheme at the relay. The NC scheme found was in turn used to help determine the achievable rates of each source, and the achievable rate of the entire system. Based on these results we then fully investigated the design of network coded multi-edge type LDPC codes. The performance of the new codes we design was investigated and shown to lead to significant improvement in BER performance relative to existing LDPC code designs for the multiple-source relaying systems with asymmetric channels.

Appendix A
Proof of Theorem 2

The graph in Fig. 2(b) can be decomposed into M sub-graphs. Each sub-graph is the Tanner graph for a source. The variable nodes in the m-th sub-graph are associated with both the digits in $\bar{\mathbf{X}}_m(\omega_{im})$ (represented by the vector $\bar{\mathbf{b}}_m$) and the effective digits for s_m in $\mathbb{C}_\oplus(\phi_{i1}, \cdots, \phi_{iM})$ (represented by the vector $\mathbf{b}_m^{eff}$). Since all the digits in $\mathbb{C}_\oplus(\phi_{i1}, \cdots, \phi_{iM})$ (represented by the vector $\mathbf{b}$) are shared by more than one source, it is not so obvious how to determine $\mathbf{b}_m^{eff}$ for s_m. Therefore, we define the m-th effective sub-graph as follows.

(1) The check nodes in the m-th effective sub-graph are the same as that in the whole graph.

(2) The variable nodes in the m-th effective sub-graph are composed of the variable nodes associated with the digits in both $\bar{\mathbf{b}}_m$ and $\mathbf{b}$.

(3) The connections between check nodes and the variable nodes in the m-th effective sub-graph are kept the same as that in the whole graph.

Then we determine the quantity of NC parity-bits that are exploited at the destination for the m-th source s_m. By this way, we can obtain the equivalent code rate of s_m in the NC scheme. Without loss of generality, we randomly pick up a parity check node c in the whole graph. Suppose there are j edges emanating from the node c. Among these edges, j_m are connected to the variable nodes associated with $\bar{\mathbf{b}}_m$, and one edge is connected to a variable node associated with $\mathbf{b}$. We have $j = \sum_{m=1}^{M} j_m + 1$, which means that there are j variable nodes sharing one bit of information provided by c.

We firstly consider the determination of the effective number if joint decoding is applied at the destination.. In the joint decoding scheme, the destination jointly decodes the received signals from the sources, *i.e.* $\bar{\mathbf{X}}_m(\omega_m^i)$, $m = 1, \cdots, M$, and the received network coded signal from the relay, *i.e.* $\mathbb{C}_\oplus(\phi_1^i, \cdots, \phi_M^i)$, the variable nodes associated with $\mathbf{b}$ belong to s_m with the probability $R_m^{1,\mathrm{nc}}/R^{1,\mathrm{nc}}$. There is $(j_m + R_m^{1,\mathrm{nc}}/R^{1,\mathrm{nc}})/j$ bit of information of c allocated to s_m. In this sense, we count the number of c as $(j_m + R_m^{1,\mathrm{nc}}/R^{1,\mathrm{nc}})/j$ in the m-th effective sub-graph. By summing all the numbers of the parity check nodes in the m-th effective sub-graph, we obtain the effective parity check nodes allocated to s_m as

$$nR_m^{1,\mathrm{nc}} = \sum_{j=1}^{d_c} \sum_{j_m=0}^{j} \frac{j_m + \frac{R_m^{1,\mathrm{nc}}}{\sum_{w=1}^{M} R_w^{1,\mathrm{nc}}}}{j} \vartheta_m^j.$$

Based on the above result, we then consider the successive decoding. In the successive decoding scheme, the destination first decodes the network coded bin index $\mathbb{C}_\oplus(\phi_1^i, \cdots, \phi_M^i)$,

then the destination decodes the sources' messages from the signals $\bar{\mathbf{X}}_m(\omega_m^i)$ for all m after the network coded signal has been canceled. In the successive decoding scheme, the network coded signal $\mathbb{C}_{\oplus}(\phi_1^i, \cdots, \phi_M^i)$ can be recovered first. Correspondingly, the black circles, *i.e.* the variable nodes associated with the digits in $\mathbb{C}_{\oplus}(\phi_1^i, \cdots, \phi_M^i)$ and the edges connected to them can be deleted from Fig. 2(b).

Since ϑ_m^j is denoted as the number of the degree-j parity check nodes which has j_m edges in the m-th effective sub-graph, the number of these parity check nodes in the m-th effective sub-graph is counted as $\vartheta_m^j(j_m + R_m^{1,\text{nc}}/R^{1,\text{nc}})/j$. As such, we can obtain the number of effective parity check nodes allocated to s_m in (4) and complete the proof. ■

REFERENCES

[1] G. Kramer, M. Gastpar, and P. Gupta, "Cooperative strategies and capacity theorems for relay networks," *IEEE Trans. Inf. Theory*, vol. 51, no. 9, pp. 3037-3063, Sep. 2005.

[2] T. M. Cover and A. A. E. Gamal, "Capacity theorems for the relay channel," *IEEE Trans. Inf. Theory*, vol. 25, no. 5, pp. 572-584, Sep. 1979.

[3] T. J. Richardson and R. L. Urbanke, "The capacity of low-density parity-check codes under message-passing decoding," *IEEE Trans. Inf. Theory*, vol. 47, no. 2, pp. 599-618, Feb. 2001.

[4] T. J. Richardson, M. A. Shokrollahi, and R. L. Urbanke, "Design of capacity-approaching irregular low-density parity-check codes," *IEEE Trans. Inf. Theory*, vol. 47, no. 2, pp. 619-637, Feb. 2001.

[5] T. J. Richardson and R. L. Urbanke, "Multi-edge type LDPC codes." Available: http://lthcwww.epfl.ch/papers/mutiledge.ps.

[6] P. Razaghi and W. Yu, "Bilayer low-density parity-check codes for decode-and-forward in relay channels," *IEEE Trans. Inf. Theory*, vol. 53, no. 10, pp. 3723-3739, Oct. 2007.

[7] M. H. Azmi and J. Yuan, "Design of multi-edge type bilayer-expurgated LDPC codes," in *Proc. IEEE International Symposium on Information Theory*, pp. 1988-1992, June 2009.

[8] A. Chakrabarti, A. de Baynast, A. Sabharwal, and B. Aazhang, "Low density parity check codes for the relay channel," *IEEE J. Sel. Areas Commun.*, vol. 25, no. 2, pp. 280-291, Feb. 2007.

[9] C. Li, G. Yue, M. A. Khojastepour, X. Wang, and M. Madihian, "LDPC-coded cooperative relay systems: performance analysis and code design," *IEEE Trans. Commun.*, vol. 56, no. 3, pp. 485-496, Mar. 2008.

[10] J. Hu and T. M. Duman, "Low density parity check codes over wireless relay channels," *IEEE Trans. Wireless Commun.*, vol. 6, no. 9, pp. 3384-3394, Sep. 2007.

[11] R. Ahlswede, N. Cai, S.-Y. R. Li, and R. W. Yeung, "Network infomation flow," *IEEE Trans. Inf. Theory*, vol. 46, no. 4, pp. 1204-1216, July 2000.

[12] T. Wang and G. B. Giannakis, "Complex field network coding for multiuser cooperative communications," *IEEE J. Sel. Areas Commun.*, vol. 26, no. 3, pp. 561-571, Apr. 2008.

[13] S. Katti, S. Gollakota, and D. Katabi, "Embracing wireless interference: analog network coding," in *Proc. ACM SIGCOMM*, Aug. 2007, pp. 397-408.

[14] S. Zhang and S.-C. Liew, "Channel coding and decoding in a relay system operated with physical-layer network coding," *IEEE J. Sel. Areas Commun.*, vol. 27, no. 5. pp. 778-796, June 2009.

[15] L. Xiao, T. E. Fuja, J. Kliewer, and D. J. Castello, "A network coding approach to cooperative diversity," *IEEE Trans. Inf. Theory*, vol. 53, no. 10, pp. 3714-3722, Oct. 2007.

[16] X. Bao and J. Li, "Adaptive network coded cooperation (ANCC) for wireless relay networks: matching code-on-graph with network-on-graph," *IEEE Trans. Wireless Commun.*, vol. 7, no. 2, pp. 574-583, Feb. 2008.

[17] C. Hausl and P. Dupraz, "Joint network-channel coding for the multiple-access relay channel," in *Proc. 3rd Annual IEEE Conference on Sensor and Ad Hoc Communications and Networks*, pp. 817-822, Sep. 2006.

[18] J. Kim, S. Park, J. Kim, Y. Kim, H. Song, "Joint LDPC codes for multi-user relay channel," in *Proc. Fourth Workshop on Network Coding, Theory and Applications*, pp. 1-6, Jan. 2008.

[19] Y. Li, G. Song, and L. Wang, "Design of joint network-low density parity check codes based on the EXIT charts," *IEEE Commun. Lett.*, vol. 13, no. 8, pp. 600-602, Aug. 2009.

[20] H. Ekström, A. Furuskär, J. Karlsson, M. Meyer, S. Parkvall, J. Torsner, and M. Wahlqvist, "Technical solutions for the 3G long-term evolution," *IEEE Commun. Mag.*, vol. 44, no. 3, pp. 38-45, Mar. 2006.

[21] S. Brink, "Convergence behavior of iteratively decoded parallel concatenated codes," *IEEE Trans. Commun.*, vol. 49, no. 10, pp. 1727-1737, Oct. 2001.

[22] S. Brink, G. Kramer, and A. Ashikhmin, "Design of low-density parity-check codes for modulation and detection," *IEEE Trans. Commun.*, vol. 52, no. 4, pp. 670-678, Apr. 2004.

[23] G. Liva and M. Chiani, "Protograph LDPC code design based on EXIT analysis," in *Proc. IEEE Global Telecommunications Conference*, pp. 3250-3254, Nov. 2007.

[24] G. Caire, G. Taricco, and E. Biglieri, "Optimum power control over fading channels," *IEEE Trans. Inf. Theory*, vol. 45, no. 5, pp. 1468-1489, July 1998.

[25] S. R. Kollu and H. Jafarkhai, "On the EXIT chart analysis of low-density parity-check codes," in *Proc. IEEE Global Telecommunications Conference*, pp. 1131-1136, Nov. 2005.

[26] E. Sharon, A. Ashikhmin, and S. Litsyn, "EXIT functions for binary input memoryless symmetric channels," *IEEE Trans. Commun.*, vol. 54, no. 7, pp. 1207-1214, July 2006.

[27] E. Sharon, A. Ashikhmin, and S. Litsyn, "Analysis of low-density parity-check codes based on EXIT functuions," *IEEE Trans. Commun.*, vol. 54, no. 8, pp. 1407-1414, Aug. 2006.

[28] "A fast and accurate degree distribution optimizer for LDPC code ensembles." Available: http://lthcwww.epfl.ch/research/ldpcopt.

Jun Li was born in 1980. He received Ph.D. degree in Electronic Engineering from Shanghai Jiaotong University, Shanghai, P. R. China in 2009. From January 2009 to June 2009, he worked in the Department of Research and Innovation, Alcatel Lucent Shanghai Bell as a Research Scientist. From June 2009 to now, he is a Research Fellow in the School of Electrical Engineering and Telecommunications, University of New South Wales, Australia. He served as the Technical Program Committee member for APCC2009, APCC2010, VTC2011 (Spring), and ICC2011. His research interests include network information theory, channel coding theory, wireless network coding and cooperative communications.

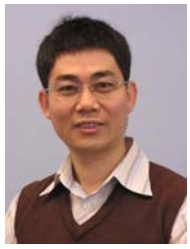

Jinhong Yuan received the B.E. and Ph.D. degrees in electronics engineering from Beijing Institute of Technology, Beijing, China, in 1991 and 1997, respectively. From 1997 to 1999 he was a Research Fellow at the School of Electrical Engineering, the University of Sydney, Sydney, Australia. In 2000 he joined the School of Electrical Engineering and Telecommunications, the University of New South Wales, Sydney, Australia, where he is currently a Professor for Telecommunications of the school. He has published two books, two book chapters and over 150 papers in telecommunications journals and conference proceedings. His list of publications is available from http://maestro.ee.unsw.edu.au/wcl/JYuan.html. His current research interests include wireless communication, communication theory, error control coding, and digital modulation.

Robert Malaney is currently an Associate Professor in the School of Electrical Engineering and Telecommunications at the University of New South Wales, Australia. He holds a Bachelor of Science in Physics from the University of Glasgow, and a Ph.D. in Physics from the University of St. Andrews, Scotland. He has over 100 publications. He has previously held research positions at Caltech, UC Berkeley - National Labs, and the University of Toronto. He is a former Principal Research Scientist at CSIRO.

Marwan Hadri Azmi received the B.Eng. degree in Electrical and Telecommunications from Universiti Teknologi Malaysia in 2003 and the M.Sc. degree in Communications and Signal Processing from Imperial College of Science, Technology and Medicine, University of London in 2005. He is now a lecturer in Universiti Teknologi Malaysia. He is currently on a study leave and working toward his Ph.D at the University of New South Wales, Australia. His research interests include communication, information and coding theory focusing on the cooperative communications and LDPC coding.

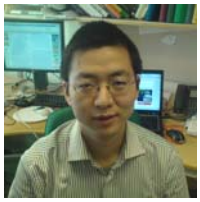

Ming Xiao (S'2002-M'2007) was born in the SiChuan Province, P. R. China, on May 22nd, 1975. He received Bachelor and Master degrees in Engineering from the University of Electronic Science and Technology of China, ChengDu in 1997 and 2002, respectively. He received Ph.D. degree from Chalmers University of technology, Sweden in November 2007. From 1997 to 1999, he worked as a network and software assistant engineer in ChinaTelecom. From 2000 to 2002, he also held a position in the SiChuan communications administration. From November 2007 to now, he has been in ACCESS Linnaeus center, school of electrical engineering, Royal Institute of Technology, Sweden, where he is currently an assistant professor. He received "Chinese Government Award for Outstanding Self-Financed Students Studying Abroad" in 2007. He received a "Hans Werthen Grant" from the Royal Swedish Academy of Engineering Science (IVA) in March 2006, and "Ericsson's Research Foundation" in 2010.